Aerosol and Air Quality Research

ORIGINAL RESEARCH
https://doi.org/10.4209/aaqr.210128

Photodegradation of Nitrogen Oxide under Solar Light Using a Facile Synthesis Catalyst

Ernso Fenelon[1,2], Sheng-Jie You[2,3], Ya-Fen Wang[2,3*]

[1] Department of Civil Engineering, Chung Yuan Christian University, Taoyuan 32023, Taiwan
[2] Department of Environmental Engineering, Chung Yuan Christian University, Taoyuan 32023, Taiwan
[3] Center for Environmental Risk Management, Chung Yuan Christian University, Taoyuan 32023, Taiwan

ABSTRACT

NO_x is becoming a hot issue due to its contribution to ozone, $PM_{2.5}$ formation, and its negative impacts on the ecosystem. In this study, the synthesis of an MgO/Bi_2S_3-BiOCl composite was carried out via the co-precipitation method for the photodegradation of nitrogen oxide (NO) under solar light. The BiOCl heterojunction is a result of interactions between the Bi_2S_3 solution and the $MgCl_2.6H_2O$ precursor. This BiOCl heterojunction provides more available active species that enhance the degradation of NO. The successful synthesis of this composite using a co-precipitation method was confirmed by different characterization analyses (XRD, FTIR, SEM, TEM, DRS, and ESR). The photocatalytic degradation of NO under solar light using 7% MgO/Bi_2S_3-BiOCl reached an efficiency of 74.6%, which was better than that obtained using pure Bi_2S_3 (42.8%) and MgO (11.2%). The reusability test showed that the 7% MgO/Bi_2S_3-BiOCl material was maintained stability in the photodegradation of NO even after five cycles. The trapping test showed that the holes (h^+) and hydroxyl ($^{\bullet}OH^-$) were the main active factors in the photodegradation process. The findings of this study confirmed that $MgCl_2.6H_2O$ is a suitable precursor leading to improvements in the performance of Bi_2S_3 for the purpose of promoting a new composite that can be used in the photodegradation of NO and could be a candidate for practical applications.

Keywords: MgO/Bi_2S_3-BiOCl, Photocatalysis, Nitrogen oxide, Solar light

Received: June 3, 2021
Revised: August 10, 2021
Accepted: August 13, 2021

* **Corresponding Author:**
yfwang@cycu.edu.tw

Publisher:
Taiwan Association for Aerosol Research
ISSN: 1680-8584 print
ISSN: 2071-1409 online

1 INTRODUCTION

NO is a harmful pollutant that is principally generated by car engines and industrial power plants. It contributes to acid rain, air pollution, and ozone depletion (Biswas and Mahajan, 2021; Biswas *et al.*, 2021; Chen *et al.*, 2017; Liu *et al.*, 2019; Wang *et al.*, 2020; Yu *et al.*, 2020). It is also responsible for the genesis of small particulate matter (PM), especially $PM_{2.5}$, which is very dangerous to human beings (Huang *et al.*, 2017; Li *et al.*, 2015; Wang *et al.*, 2016; Zhao *et al.*, 2016). Many methods have been applied to reduce and control the effects of NO in the environment, including denitrification of NO_x emissions, (de-NO_x) technologies (Yan *et al.*, 2018), electron beam irradiation, adsorption, wet absorption, selective catalytic reduction (SCR), and selective non-catalytic reduction (Yan *et al.*, 2018). In addition to all the remediation methods, the use of a photocatalyst is a process of generating energy by using chemical reactions with light energy at an optimum point for the purpose of degrading environmental pollutants (Fenelon *et al.*, 2019; Feng *et al.*, 2019; John *et al.*, 2021; Neves *et al.*, 2017) and is regarded as a "clean" and productive process (Nguyen *et al.*, 2019).

When applying a high-quality catalytic, it is necessary to obtain better performance at low temperatures and to reduce application costs (Zhang *et al.*, 2020). Both conventional and developing catalysts, such as TiO_2, ZnO, SnO_2, Cu_2O, Bi_2S_3, g-C_3N_4, Bi_2WO_6, and $BiPO_4$, among others, are typically applied for the reduction of environmental pollutants, including NO (Li *et al.*, 2019; Nguyen *et al.*,

2019). Unfortunately, their performance is usually limited either by a large band-gap or rapid photogeneration of recombination electrons (e^-) and holes (h^+). Some studies in the previous literature on this topic also suggest limitations in these catalysts due to low degradation of NO under visible light, solar light, and UV light. A new photocatalyst is therefore needed to improve the photodegradation of NO. Among various available catalysts, Bi_2S_3 is an excellent semiconductor that has drawn broad attention related to thermoelectric devices (Guo *et al.*, 2013), super capacitor electrodes (Nie *et al.*, 2015), sensors (Sun *et al.*, 2016), solar cells (Li *et al.*, 2016), and Schottky diodes (Bao *et al.*, 2008). Additionally, photocatalysts based on Bi_2S_3 are very appealing for the following reasons: (1) The narrow band-gap implies broad photo-absorption ability, which is favored for photocatalytic activity, and (2) raw resources including bismuth and sulfide are plentiful at the global level and thus easily accessible at a low cost. However, pure Bi_2S_3 is limited in terms of achieving high performance in the conversion of solar energy because of its small optical band-gap (1.3 eV) and thus has been restricted to the easy recombination of photogenerated e^-–h^+ pairs (Long *et al.*, 2015).

To overcome the above-reverenced problems related to the photocatalytic efficiency of Bi_2S_3 under solar light, an MgO material was applied as a new companion to improve the performance of Bi_2S_3. In this study, MgO was selected because of its low heat power and because it is chemically inert, has high optical clarity, and is thermally stable (Gao *et al.*, 2012). In addition, the presence of the BiOCl compound leads to a heterojunction that typically forms in the preparation of a Bi_2S_3 material with a precursor that contains Cl ions in water solvent (Fenelon *et al.*, 2020; Guan *et al.*, 2013; Lei *et al.*, 2009; Zhang *et al.*, 2014). Therefore, the MgO/Bi_2S_3-BiOCl composite discussed in this work was developed in a solution of Bi_2S_3 with the $MgCl_2.6H_2O$ precursors in water, and its efficacy was successfully confirmed using a characterization analysis. Additionally, the presence of BiOCl was found to be beneficial for photocatalytic activities due to the availability of more active species leading to the generation of electron-hole pairs and the fact that it enhances the performance of the composite. This study involves taking advantage of this composite, which is synthesized for the first time using a co-precipitation method for potential application in the photodegradation of NO assisted by solar light.

2 MATERIALS AND METHOD

2.1 Materials and Chemicals

Xilong Chemical Co., Ltd., Beijing, China, provided the bismuth nitrate ($Bi(NO_3)3H_2O$) chemical at a weight fraction of 0.990. Magnesium Chloride Hexahydrate (BioXtra, $\geq$ 99.0%), isopropyl alcohol (IPA, Merck, 99.99%), ethanol (C_2H_6O), sodium hydroxide (NaOH, 99%), Thiourea (CH_4N_2S, China, 99.9%) were utilized in this study, as well as double-distilled water (DDW).

2.2 Synthesis of Bi_2S_3, MgO Nanoparticles, and MgO/Bi_2S_3-BiOCl Composites

The co-precipitation method was used to synthesize all of the catalysts. The Bi_2S_3 catalyst was prepared by mixing 5.174 g of Bi $(NO_3)_3.5H_2O$ and 133.34 ml of double-distilled water (DDW), after which 1.2 g of CH_4N_2S was applied in 13.34 ml of DDW separately mixed for 30 min. After the mixing time, a thiourea solution was introduced into the solution of $Bi(NO_3)_3.5H_2O$ and constantly mixed for 60 min. Afterward, a yellow solution was recovered and washed at least four times using DDW and C_2H_6O at a ratio of 5:1 to remove all of the impurities. Finally, the Bi_2S_3 sample was dried at 60°C for 12 hours and then calcinated at 400°C for 2 hours.

Synthesis of the MgO material was carried out using the same precipitation method. 5.1 g of $MgCl_2.6H_2O$ was put into a mixed solution of 80 mL of DDW. After that, the NaOH solutions were added to adjust the solution to pH 10 for the purpose of facilitating the oxidation of magnesium, after which it was mixed for 2 hours. Finally, the substance was rinsed with ethanol and DDW, dried at 60°C for 12 hours, and then calcined at 400°C for 2 hours.

Synthesis of the MgO/Bi_2S_3-BiOCl composites (Fig. 1) was carried out using different weight percentages of MgO and Bi_2S_3 (5%, 7%, 10%, and 15% MgO). A solution of synthesized MgO was added dropwise into the Bi_2S_3 solution and mixed for 3 hours. Finally, the material was washed four times with C_2H_6O and DDW, centrifuged, dried at 60°C for 12 hours, and then calcinated at 400°C for 2 hours.

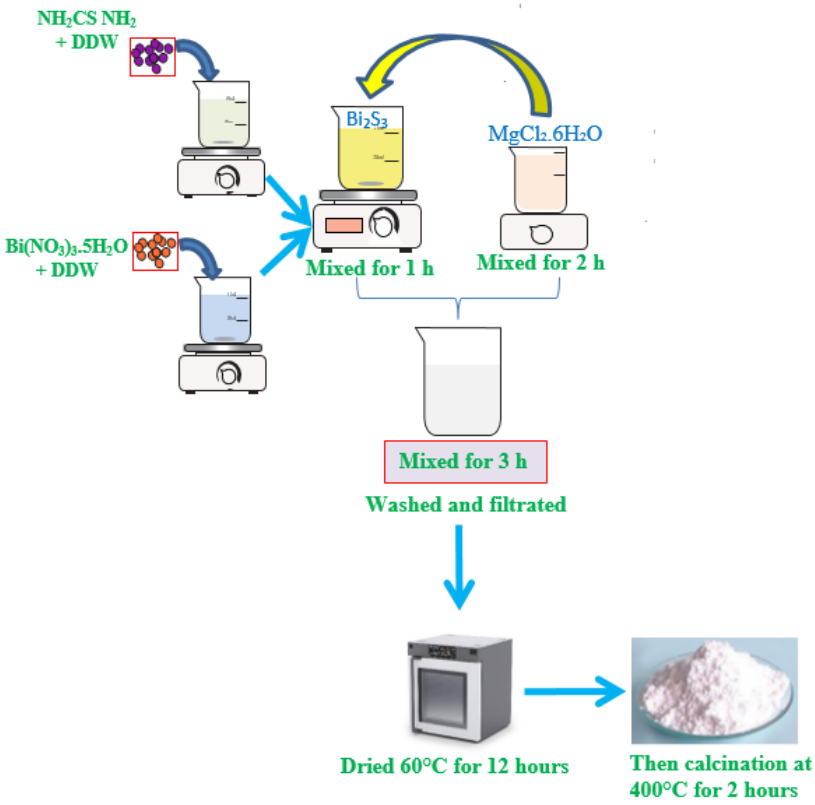

Fig. 1. Synthesis of the MgO/Bi_2S_3-BiOCl composites.

2.3 Surface Analysis

Scanning and transmission electron microscopy (SEM, TEM) were applied to study the morphology of the materials. The crystal structure and phase composition were analyzed using an X-ray diffraction (XRD) pattern on a Bruker D8-Advance 5005 with Cu K radiation of 0.154064 nm. The feature group and bonding of the catalyst were calculated using Fourier transform infrared spectroscopy (FTIR). Using a UV-Vis spectrometer, the optical properties of the composites were determined using UV-vis diffuse reflectance spectroscopy (DRS) in a wavelength range of 200–800 nm (JASCO-V550). Using a Bruker EMX Plus X-Band spectrometer, the electron spin resonance (ESR) with DMPO (5,5-Dimethyl-1-Pyrroline N-oxide) was used to analyze the ESR signals of the reactive oxygen species (ROSs) produced in the photodegradation activity, and Malvern Panalytical's Zetasizer Nano ZS was used to determine the particle size of the preparation material.

2.4 Pollutant Photocatalytic Degradation Measurements

The photocatalytic activity of the material shown in Fig. 2 was assessed by analyzing the photodegradation potential of nitrogen oxide using 500 ppb with a continuous flow reactor set at 3 L min^{-1} at room temperature. A 300 W Xenon lamp 135 (Perfect Light MICRO SOLAR 300, Beijing, China) was used for solar light irradiation. 0.20 g of the photocatalysts were added to 20 mL of DDW and transferred to a glass dish (d = 12 cm), followed by drying at 80°C and placing in the center of the reactor. After the catalyst reached adsorption/desorption balance at 480 ppb, the lamp was turned on while maintaining a humidity of 40%. A NO_x analyzer was continuously used to track the concentration of NO. The NO degradation was calculated using C/C0, in which C represents the current NO concentration in the exit, and C0 is the original NO contamination. For the trapping test, different scavengers of 10^{-3} M were added to the catalyst. Potassium iodide (KI), isopropyl alcohol (IPA), and potassium dichromate ($K_2Cr_2O_7$) were used as effective scavengers of the holes, hydroxyl radicals, and photogenerated electrons, respectively, in this procedure. The kinetics $K = (\ln(C/C_0))/t$ of the photocatalysts were measured using the obvious first-order rate constant k (min^{-1}) of NO (ppbV) at the initial C0, and C is the final concentration at different time (min) (Pham *et al.*, 2020).

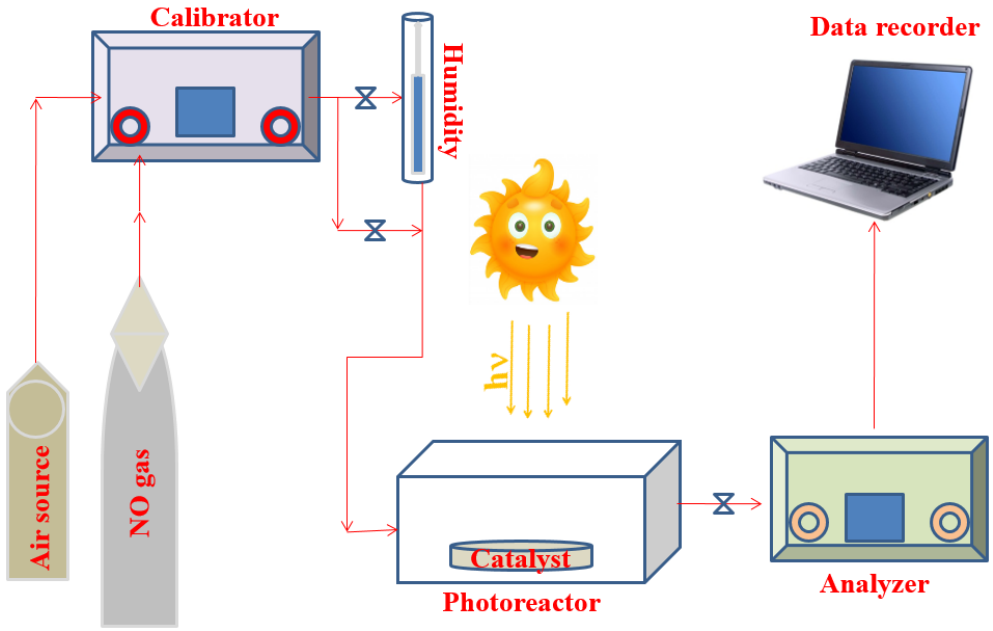

Fig. 2. Photodegradation of NO.

3 RESULTS AND DISCUSSION

3.1 XRD Pattern Analysis

The XRD analysis of MgO, Bi_2S_3, and MgO/Bi_2S_3-BiOCl is shown in Fig. 3. The Bi_2S_3 pattern was matched to the orthorhombic phase JCPDS No. 170320; the peaks at 23.8°, 28.28°, 31.86°, 34.65°, 41.17°, 45.52°, 47.73°, 54.47°, and 58.46° are related to planes (101), (211), (221), (311), (430), (440), (501), (360), and (640), respectively. The MgO NPS presented by the cubic MgO phase (PDF-00-004-0829) with diffraction peaks at 36.95°, 42.91°, 62.31°, 74.69°, and 78.55° are correlated with planes (111), (200), (220), (311), and (222), respectively, indicate that the precursors of MgO are high levels of crystalline. The typical diffraction peaks of BiOCl detected in the composite were found in the JCPDS, no. 06-0249 phase. The existence of BiOCl was confirmed in a previous report, which clarified that the formation of a BiOCl heterojunction occurs when Bi_2S_3 is mixed with $MgCl_2.6H_2O$ precursor in water. The XRD patterns analysis successfully confirmed the easy synthesis of the MgO/Bi_2S_3-BiOCl material for photocatalytic activities.

3.2 Fourier Transform Infrared Spectroscopy (FTIR) Spectra

The FTIR analysis in the solid phase was carried out using the KBr pellet procedure in a 400−4000 cm^{-1} area to verify the existence of functional groups and the chemical bonding of the materials. Fig. 4 illustrates the FTIR analysis of MgO, Bi_2S_3, and the MgO/Bi_2S_3-BiOCl material. The prominent peaks at around 528 cm^{-1} and 1155 cm^{-1} are related to the Bi-O and Bi-Cl stretching modes, respectively, implying the presence of highly pure BiOCl (Seddigi *et al.*, 2017). The vibration at 617 cm^{-1} is connected to C–S, and the formation of Bi^{3+} indicates C–N stretching (Jayachandhiran *et al.*, 2017). The vibrational mode centered at 842 cm^{-1} was attributed to Bi–S stretching (Cao *et al.*, 2018). The regions between 1350 cm^{-1} to 1450 cm^{-1} may have been responsible for the Bi-S vibration. The band at 1382 cm^{-1} was caused by the bending vibration of Mg-O (Essien *et al.*, 2020; Viswanatha *et al.*, 2012), and the vibration at around 3400 cm^{-1} corresponded to the O-H vibration from the water used in the preparation of the material (Zhao *et al.*, 2018). The wavelength at 3421 cm^{-1} was associated with the O-H vibration in alcohol (Dobrucka, 2018; Essien *et al.*, 2020). The band at 3699 cm^{-1} was due to the formation of MgO NPs (Ansari *et al.*, 2018). These functional group vibrations proved that the MgO NPs, Bi_2S_3 nanorods, and MgO/Bi_2S_3-BiOCl composite were successfully synthesized. The FTIR results also confirmed the formation of BiOCl, which was also observed in the XRD analysis spectra.

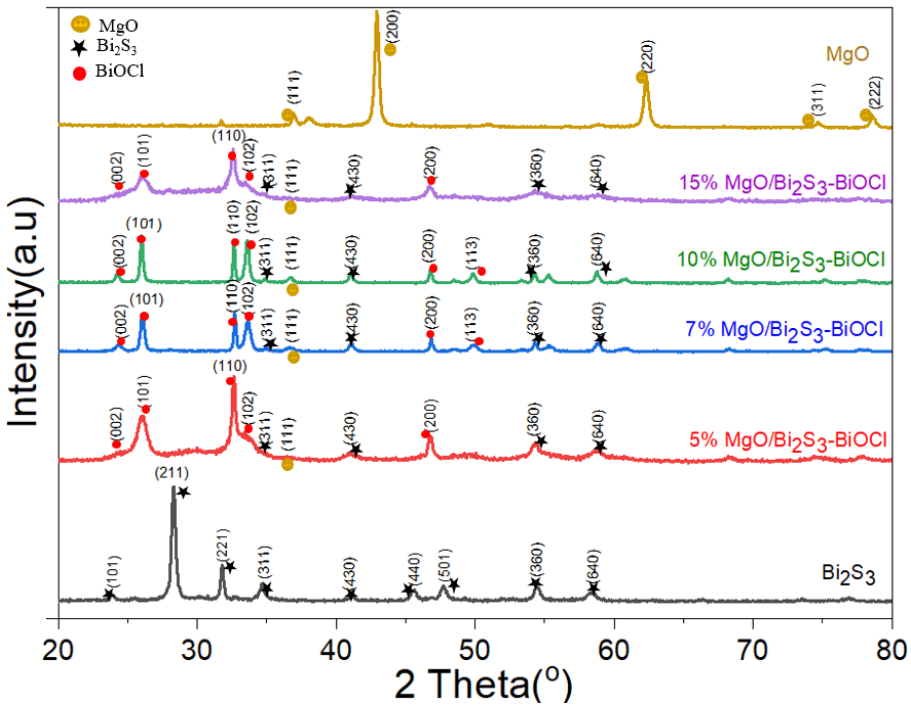

Fig. 3. XRD pattern analysis of the MgO, Bi_2S_3, and MgO/Bi_2S_3-BiOCl materials.

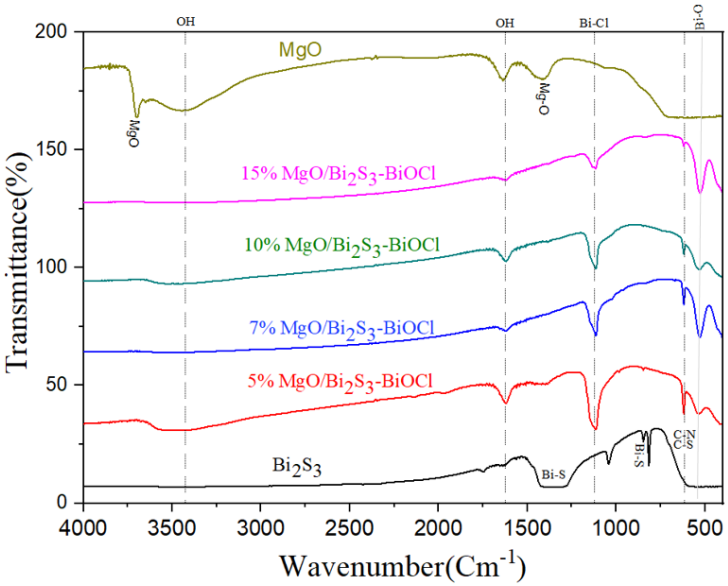

Fig. 4. FTIR analysis of Bi_2S_3, MgO, and MgO/Bi_2S_3-BiOCl.

3.3 The Morphology of MgO/Bi_2S_3-BiOCl

The surface morphology of the Bi_2S_3, MgO, and MgO/Bi_2S_3-BiOCl composites was examined using scanning electron microscopy (SEM). As shown in Figs. 5 (a) and 5(b), the particle sizes of the Bi_2S_3 and MgO samples are irregular. Figs. 5(c–f) show that the MgO/Bi_2S_3-BiOCl material at a 5%, 7%, 10%, and 15% weight of MgO, respectively, are smoother and could thus provide a better performance in the photocatalytic process. The increase in the MgO content on the surface of Bi_2S_3 indicated the growth of particles in the form of a branched structure, which may have been due to the growth of MgO nanoparticles over the surface of the Bi_2S_3 leading a more active species that served to catch the photo-induced electrons. Otherwise, the excess amount of MgO content converted the pores of the catalyst, so the defects became recombination centers

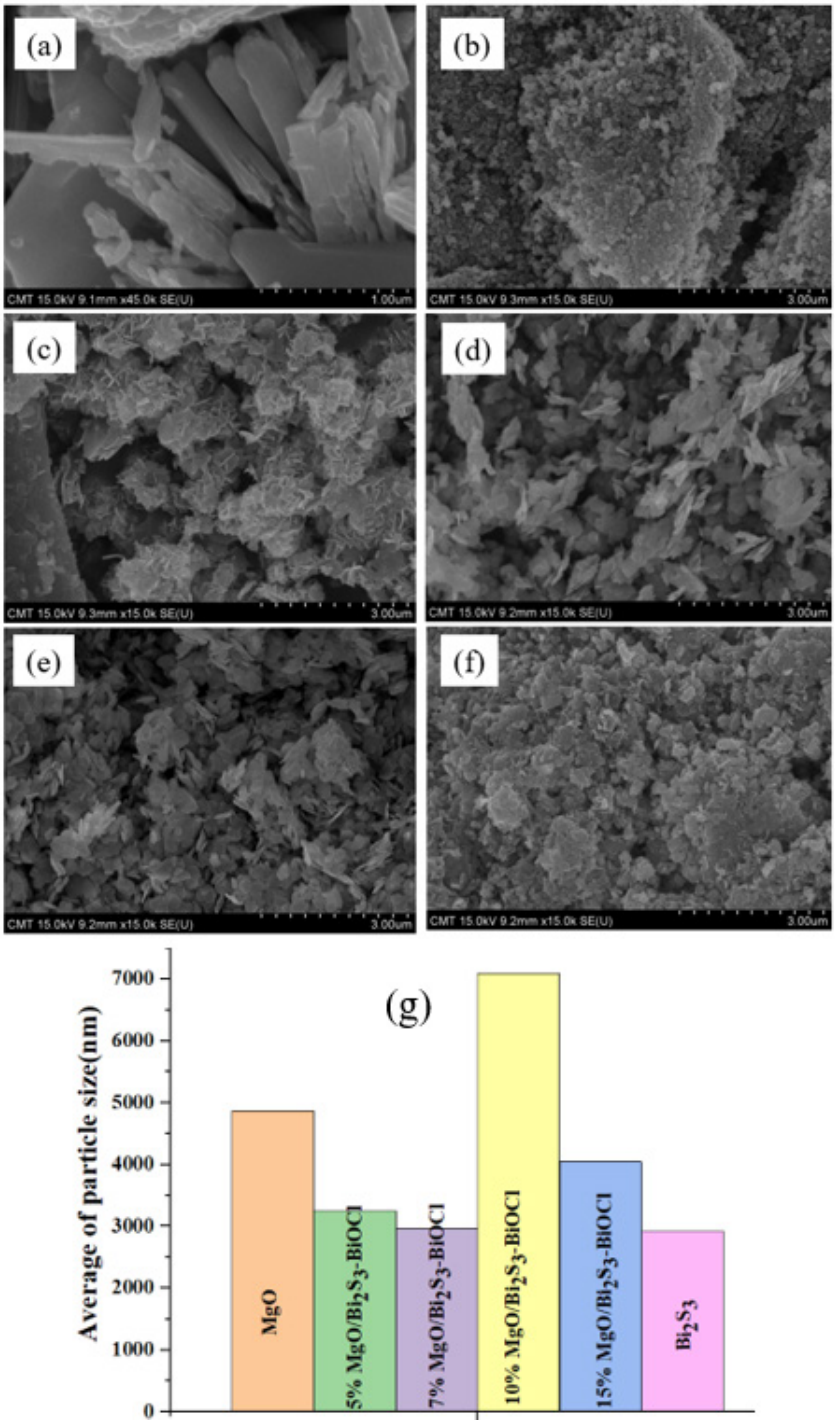

Fig. 5. Scanning electron microscopy image of (a) Bi_2S_3, (b) MgO, (c) 5% MgO/Bi_2S_3-BiOCl, (d) 7% MgO/Bi_2S_3-BiOCl, (e) 10% MgO/Bi_2S_3-BiOCl, and (f) 15% MgO/Bi_2S_3-BiOCl composites (g) average particle size.

and reduced the photodegradation ability of the composite. The particle size of the material was also measured using Malvern Panalytical's Zetasizer Nano ZS to study the influence of particle size on the photocatalytic degradation of NO. The results shown in Fig. 5(g) indicate that the average particle sizes of Bi_2S_3, MgO, 5% MgO, 7% MgO, 10% MgO, and 15% MgO were 2927 nm, 4871 nm, 3251 nm, 2963 nm, 7093 nm, and 4046 nm, respectively. The formation of BiOCl could have cause the increase in the particle size of the material (Bárdos *et al.*, 2021). Fig. 6(a) presents the transition electron microscopy (TEM) morphology of Bi_2S_3 nanorods synthesized using a

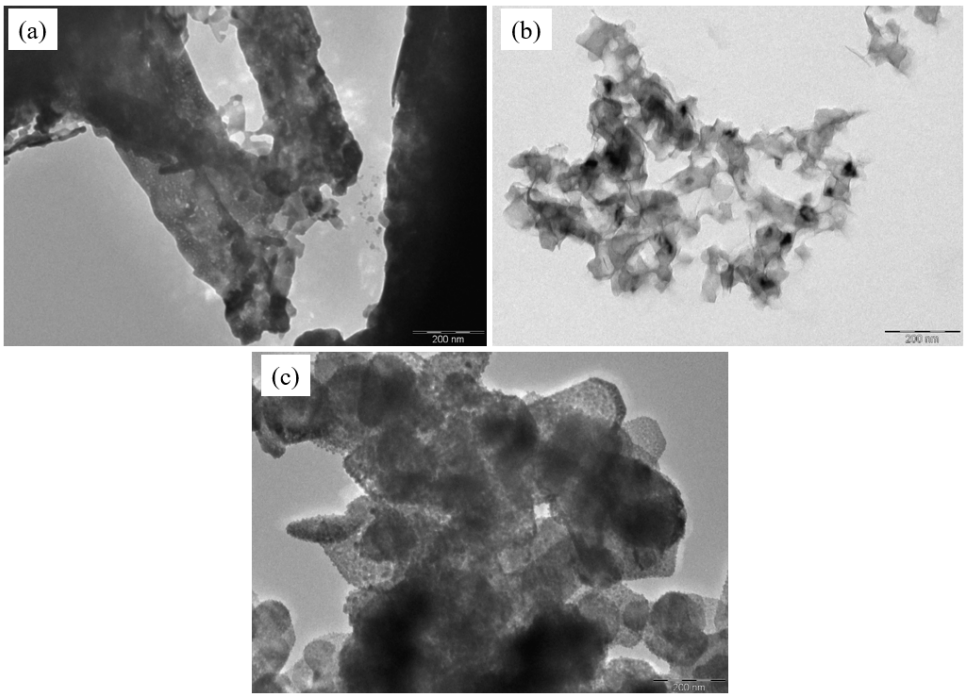

Fig. 6. Transition electron microscopy (TEM) morphology of Bi_2S_3, MgO, and 7% MgO/Bi_2S_3-BiOCl.

simple precipitation method. The MgO NPs are shown in Fig. 6(b), where the nanoparticles in the image are uniform in size. Fig. 6(c) shows that the morphology of the composite preparation with the doping of the $MgCl_2.6H_2O$ precursor on the Bi_2S_3 solution is very different compared to the pure MgO and Bi_2S_3, which confirmed the formation of the new composite MgO/Bi_2S_3-BiOCl detected in the XRD pattern. Therefore, the characterization of the as-prepared material successfully confirmed the synthesis of the MgO/Bi_2S_3-BiOCl composites using the simple co-precipitation method proposed in this work.

3.4 Diffuse Reflectance Spectroscopy (DRS) Analysis

The diffuse reflection spectra (DRS) were used to examine the light absorption behavior of the material at wavelengths ranging between approximately 250 and 800 nm (Fig. 7). The MgO material exhibits a large wavelength of around 300 nm, which means it can only work under UV light. The Bi_2S_3 materials showed the full wavelength of 800 nm, which could be applied easily

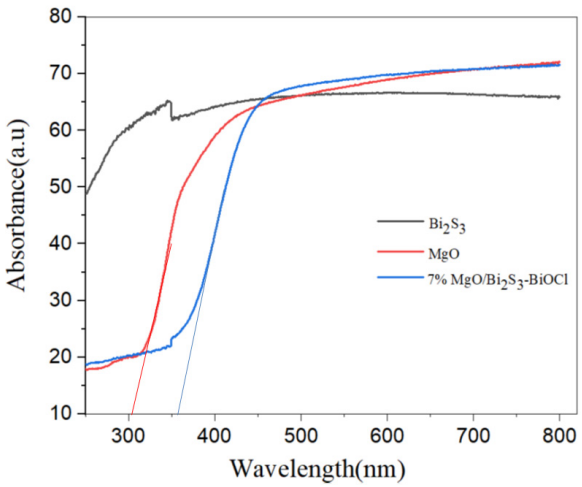

Fig. 7. Diffuse reflectance spectroscopy analysis of Bi_2S_3, MgO, and MgO/Bi_2S_3-BiOCl.

using visible light. In the case of the MgO/Bi_2S_3-BiOCl material, as a result of the Bi_2S_3 and MgO in the synthesis process, a wavelength of approximately 350 nm appeared between the visible light and UV-light area, so the DRS analysis confirmed that this composite can exhibit better performance under solar light than the pure Bi_2S_3 and MgO.

3.5 NO degradation Using MgO, Bi_2S_3, and MgO/Bi_2S_3-BiOCl under Solar Light Irradiation

Fig. 8(a) shows the photocatalytic performance of Bi_2S_3, MgO, and MgO/Bi_2S_3-BiOCl for a 30-minute period under solar light irradiation. The NO degradation efficiency of Bi_2S_3, MgO, 5% MgO/Bi_2S_3-BiOCl, 7% MgO/Bi_2S_3-BiOCl, 10% MgO/Bi_2S_3-BiOCl, and 15% MgO/Bi_2S_3-BiOCl were 42.8%, 11.2%, 66.4%, 74.6%, 58%, and 50.3% respectively. The results showed that increasing the amount of MgO doped on Bi_2S_3 from 5% to 7% increased the removal of NO, but the performance of the composite was decreased with increases in the amount of MgO of more than 7% because an excessive amount of MgO can turn the composite to the UV area. However, solar light has less than a 5% UV irradiation, so the excess amount of pure MgO had poor performance under solar light. In addition, when the amount of MgO was optimal or less than optimal, the MgO acted as a photo-induced electron capture center. However, When the weight of the MgO was greater than its maximum value, the reabsorption of photo-induced e^- and h^+ in the material

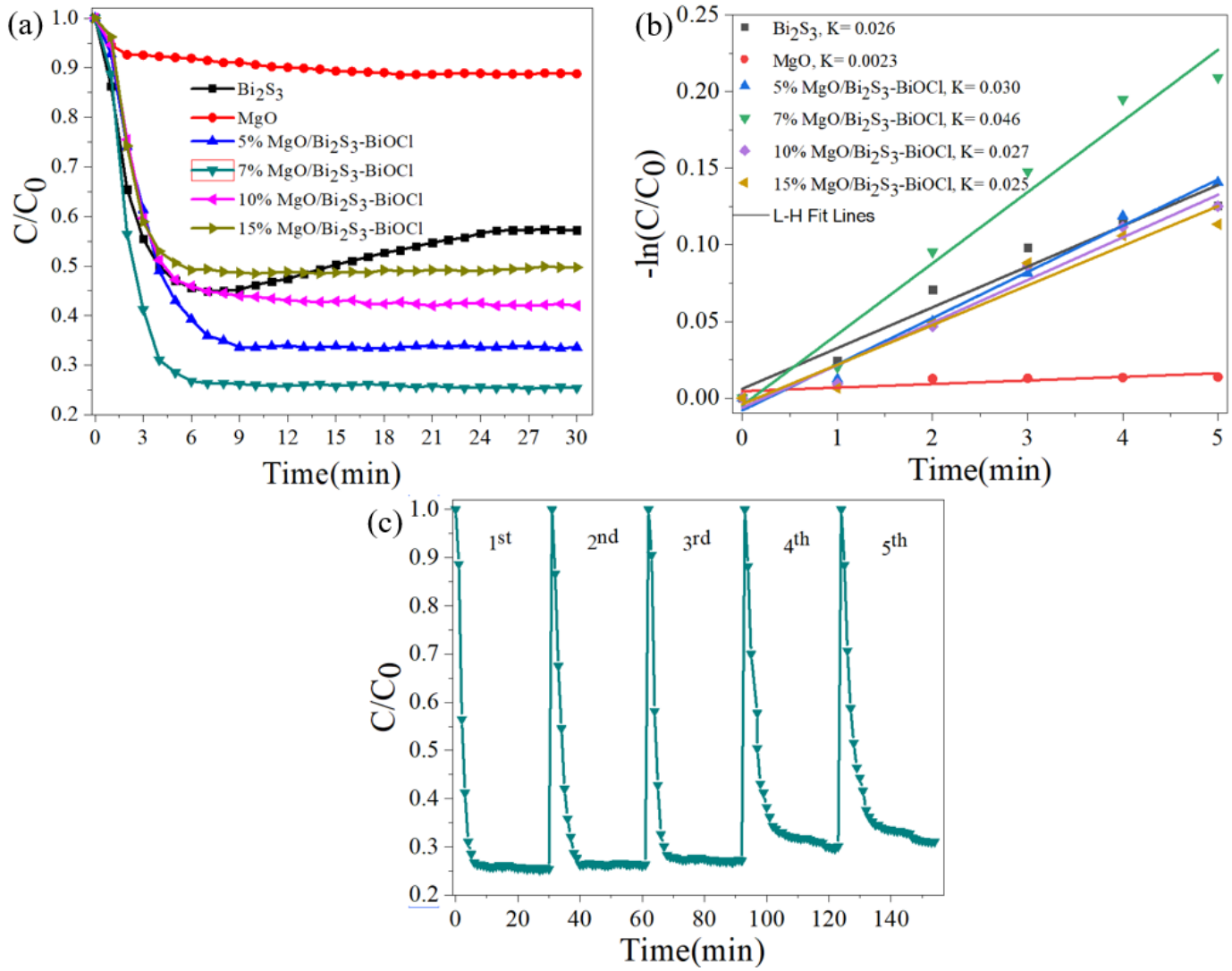

Fig. 8. Nitrogen oxide degradation by MgO, Bi_2S_3 and MgO/Bi_2S_3-BiOCl under (a) solar light irradiation, (b) L–H fit Lines, and reusability test of (c) 7% MgO/Bi_2S_3-BiOCl.

Table 1. Comparison of previous studies on the photocatalytic degradation of NO.

Catalysts	NO Concentration(ppb)	Light sources	Removal efficiency (%)	References
TiO_2/graphene	1000	UV light	52.28	(Trapalis *et al.*, 2016)
SnO_2	500	Solar light	63.37	(Huy *et al.*,2018)
TiO_2/graphene	1000	Visible light	24.05	(Trapalis *et al.*, 2016)
Ag/LDH	400	Solar light	43	(Zhu *et al.*, 2017)
Cr/ZnO	500	Visible light	24.44	(Nguyen *et al.*, 2019)
La/TiO_2	500	Solar light	32	(Huang *et al.*, 2017b)
Pd/F-TiO_2	1000	Solar light	52	(Fujiwara *et al.*, 2016)
Bi/BiOI/$(BiO)_2CO_3$	550	Visible light	50.7	(Sun *et al.*, 2019)
Ag@Bi_2S_3	500	Solar light	31.12	(Pham *et al.*, 2021)
w-Pd/c-TiO_2	1000	Solar light	55	(Fujiwara *et al.*, 2016)
B,N-doped TiO_2	400	Visible light	53	(Ding *et al.*, 2011)
f-Pd/TiO_2	1000	Solar light	63.5	(Fujiwara *et al.*, 2016)
SnO_2/PANI	450	Solar light	16	(Bui *et al.*, 2018)
MgO/Bi_2S_3-BiOCl	500	Solar light	74.61	This study

increased and led to poor degradation of the pollutant (Guo *et al*., 2012). In addition, the average particle size of the composite material showed that the 7% MgO/Bi_2S_3-BiOCl had the lowest particle size, which led to an increase the surface area available for producing more active species and in turn, to better degradation of NO under solar light. A comparison with some previous publications is provided in Table 1, which shows that the photodegradation of nitrogen oxide is limited under visible light, solar light, and even UV light. Therefore, in the present study, the new, efficient MgO/Bi_2S_3-BiOCl composites applied for the first time for photocatalytic degradation of nitrogen oxide, showed significant results under solar light. The comparison also shows that the MgO/Bi_2S_3-BiOCl composites for degradation of NO are very competitive and may be candidates for practical application. The Fig. 8(b) indicated that the reaction rates (k) of the Bi_2S_3, MgO, 5% MgO/Bi_2S_3-BiOCl, 7% MgO/Bi_2S_3-BiOCl, 10% MgO/Bi_2S_3-BiOCl, and 15% MgO/Bi_2S_3-BiOCl were 0.026, 0.0023, 0.030, 0.046, 0.027, and 0.025, respectively, which indicates that the 7% MgO/Bi_2S_3-BiOCl exhibited the highest degradation rate. Furthermore, due to the method used to synthesize MgO/Bi_2S_3-BiOCl, the components at the BiOCl heterojunction could not be separates from the composite to measure their individual performance in the photodegradation activities of NO. The stability of the photocatalyst, as shown in Fig. 8(c), was studied to evaluate the reusability of using the 7% MgO/Bi_2S_3-BiOCl material. The result showed that the photocatalytic degradation of NO remained stable after five cycles, implying that the photocatalyst was highly stable throughout the photodegradation process.

3.6 Trapping Test, DMPO-ESR Spectra, and Photodegradation Mechanism of NO Using MgO/Bi_2S_3-BiOCl under Solar Light

The trapping experiment was conducted to determine the main active factor contributing to the photodegradation of nitrogen oxide using MgO/Bi_2S_3-BiOCl by confirming its photocatalytic mechanism under solar light. Fig. 9(a) shows that the removal efficiency of NO was slightly decreased by the addition of 10^{-3} M of potassium dichromate ($K_2Cr_2O_7$) (a quencher of $\bullet O_2^-$), but significantly decreased by adding isopropanol (IPA) (a quencher of $^{\bullet}OH$) and potassium iodide (KI) (a quencher of h^+). Therefore, the results show that the h^+ and OH radicals of the MgO/Bi_2S_3-BiOCl composite are the main factors contributing to the photodegradation of NO under solar light.

To understand the potential of the production of reactive oxygen species, the trapping test was conducted using electron spin resonance of a 7% MgO/Bi_2S_3-BiOCl material for 12 minutes with 5,5-Dimethyl-1-Pyrroline N-oxide (DMPO-ESR) (ROS). The results in Fig. 9(b) reveal that under dark conditions, there is almost no signal for (DMPO-•OH), and (DMPO-O_2^-). After the light was turned on, active vibration was detected. The results explain that the generated OH radicals came from the holes (h^+) and facilitated the oxidation of nitrogen oxide.

The mechanism of the degradation of NO by MgO/Bi_2S_3-BiOCl under solar light can be described by the following reactions: Eq. (1) explains that the holes stay in the valence band (VB), and the

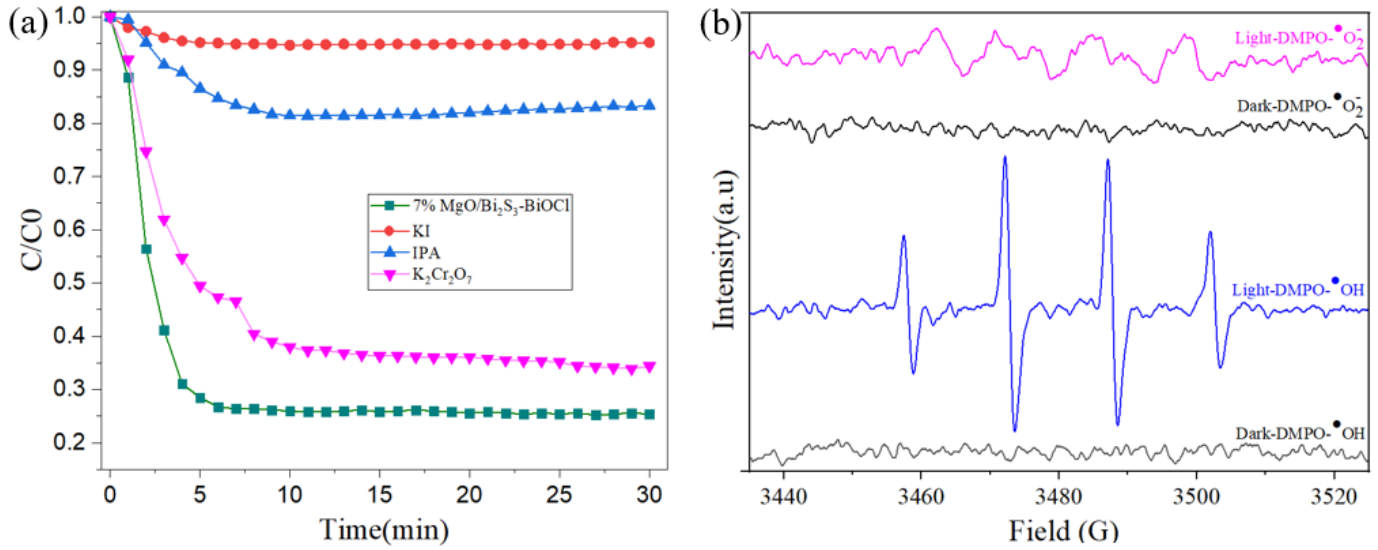

Fig. 9. (a) Active species trapping test, (b) DMPO-ESR spectra of 7% MgO/Bi_2S_3-BiOCl.

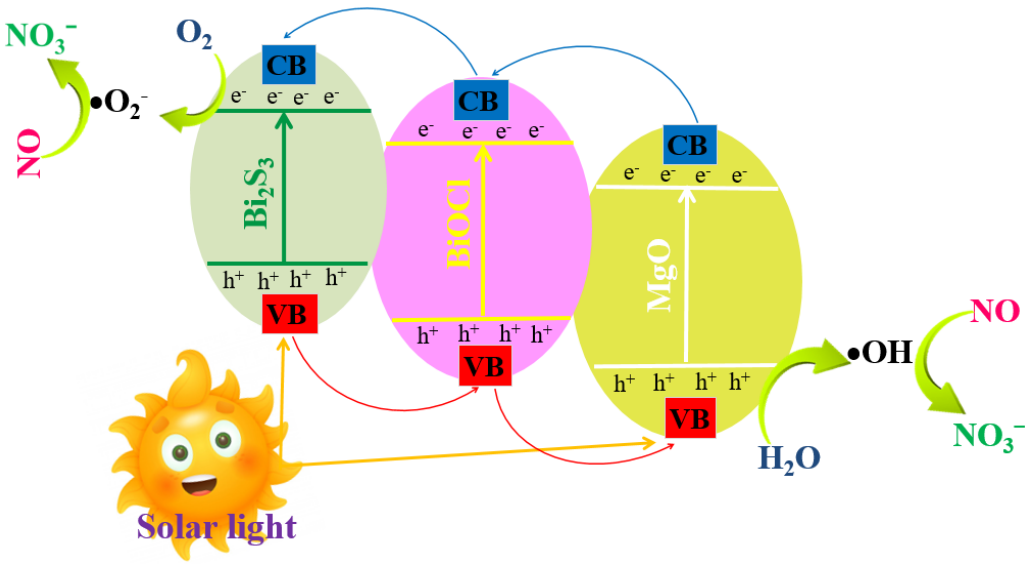

Fig. 10. Mechanism of NO photocatalytic degradation using MgO/Bi_2S_3-BiOCl.

excited electrons move from the valence band (VB) to the conduction band (CB). The electron-hole couples travel to the surface of the MgO/Bi_2S_3-BiOCl. Eq. (2) explains that the electrons then combine with oxygen to form $^{\bullet}O_2$. In Eq. (5), $^{\bullet}OH$ forms by the combination of holes (h^+) with the OH^- from Eqs. (3) and (4). In Eq. (6), $^{\bullet}OH$ forms when the holes react with water.

In terms of Eqs. (7) and (9), Fig. 10 shows that both $\bullet O_2^-$ and •OH reacted and degraded NO into NO_3, and the ESR spectra and the trapping analysis shown in Fig. 9 explain that $\bullet O_2^-$ and •OH are used for the photocatalytic degradation of NO under solar light.

$$MgO/Bi_2S_3\text{-}BiOCl + hv \longrightarrow MgO/Bi_2S_3\text{-}BiOCl\ (h^+VB + e^-CB) \quad (1)$$

$$O_2 + e^-CB \longrightarrow \bullet O^-_2 \quad (2)$$

$$H_2O + \bullet O_2^- + \longrightarrow OH^- + \bullet HO_2 \quad (3)$$

$$\bullet HO_2 + H_2O + e^- \longrightarrow H_2O_2 + OH^- \quad (4)$$

$h^+ + OH^- \rightarrow \bullet OH$ (5)

$H_2O + h^+ \rightarrow HO\bullet + H^+$ (6)

$NO + \bullet O_2^- \rightarrow NO^-_3$ (7)

$NO + 2HO\bullet \rightarrow NO_2 + H_2O$ (8)

$NO_2 + \bullet OH \rightarrow NO_3^- + H^+$ (9)

4 CONCLUSIONS

This research was focused on introducing a new, efficient photocatalyst (MgO/Bi_2S_3-BiOCl) for the purpose of reducing the fast recombination of electron-hole pairs during the degradation of nitrogen oxide under solar light.

The surfaces analysis confirmed that the MgO/Bi_2S_3-BiOCl composite was successfully synthesized using the easy method proposed in this work.

The results showed that only 7% MgO was doped on Bi_2S_3, which indicates optimum removal efficiency and a higher degradation rate. Furthermore, the 7% MgO/Bi_2S_3-BiOCl composite also had the smallest particle size, which contributed to increasing the surface area of the composite and leading to better degradation of NO.

The formation of BiOCl in the composite improved the active species and led to better photodegradation of NO under solar light irradiation. The photodegradation efficiency of NO with the application of 7% MgO/Bi_2S_3-BiOCl was around 1.75 times higher than was the case for the pure Bi_2S_3.

The trapping test and DMPO-ESR spectra showed that the holes (h^+) and the OH radicals were the main factors contributing to the photodegradation of NO when solar light was applied to the compound of 7% MgO/Bi_2S_3-BiOCl.

The photocatalytic degradation results also showed that the pure Bi_2S_3 was unstable during the degradation process, and the presence of the MgO doped on the Bi_2S_3 led to good stability even after five recycles.

Additionally, the MgO/Bi_2S_3-BiOCl composite is very competitive compared to the degradation of NO in the previous studies. Finally, the use of precursors that contain Cl ion are suggested to improve the performance of Bi_2S_3 by promoting more active species in the photodegradation of environmental pollutants for practical applications.

ACKNOWLEDGEMENT

A special thanks to Chung Yuan Christian University for supporting this work through project number: 109609432.

DSICLAIMER

This present manuscript has no financial interests in completing

REFERENCES

Ansari, A., Ali, A., Asif, M., Shamsuzzaman, S. (2018). Microwave-assisted MgO NP catalyzed one-pot multicomponent synthesis of polysubstituted steroidal pyridines. New J. Chem. 42, 184–197. https://doi.org/10.1039/C7NJ03742B

Bao, H., Li, C.M., Cui, X., Gan, Y., Song, Q., Guo, J. (2008). Synthesis of a highly ordered single-crystalline Bi_2S_3 nanowire array and its metal/semiconductor/metal back-to-back schottky diode. Small 4, 1125–1129. https://doi.org/10.1002/smll.200800007

Bárdos, E., Márta, V.A., Fodor, S., Kedves, E.Z., Hernadi, K., Pap, Z. (2021). Hydrothermal

crystallization of bismuth oxychlorides (BiOCl) using different shape control reagents. Materials 14, 2261. https://doi.org/10.3390/ma14092261

Biswas, M.S., Mahajan, A.S. (2021). Year-long concurrent MAX-DOAS observations of nitrogen dioxide and formaldehyde at pune: Understanding diurnal and seasonal variation drivers. Aerosol Air Qual. Res. 21, 200524. https://doi.org/10.4209/aaqr.200524

Biswas, M.S., Pandithurai, G., Aslam, M.Y., Patil, R.D., Anilkumar, V., Dudhambe, S.D., Lerot, C., De Smedt, I., Van Roozendael, M., Mahajan, A.S. (2021). Effect of boundary layer evolution on nitrogen dioxide (NO_2) and formaldehyde (HCHO) concentrations at a high-altitude observatory in western India. Aerosol Air Qual. Res. 21, 200193. https://doi.org/10.4209/aaqr.2020.05.0193

Bui, P.D., Tran, H.H., Kang, F., Wang, Y.F., Cao, T.M., You, S.J., Vu, N.H., Pham, V.V. (2018). Insight into the photocatalytic mechanism of tin dioxide/polyaniline nanocomposites for NO degradation under solar light. ACS Appl. Nano Mater. 1, 5786–5794. https://doi.org/10.1021/acsanm.8b01445

Cao, J.T., Wang, B., Dong, Y.X., Wang, Q., Ren, S.W., Liu, Y.M., Zhao, W.W. (2018). Photogenerated hole-induced chemical redox cycling on $Bi_2S_3/Bi_2Sn_2O_7$ heterojunction: Toward general amplified split-type photoelectrochemical immunoassay. ACS Sens. 3, 1087–1092. https://doi.org/10.1021/acssensors.8b00332

Chen, L., Zheng, C., Gao, X., Cen, K., Bao, K., Li, K., Lv, B., Bao, Z., Lin, C., Wu, X. (2017). Ozone and secondary organic aerosol formation of toluene/NO_x irradiations under complex pollution scenarios. Aerosol Air Qual. Res. 17, 1760–1771. https://doi.org/10.4209/aaqr.2017.05.0179

Ding, X., Song, X., Li, P., Ai, Z., Zhang, L. (2011). Efficient visible light driven photocatalytic removal of NO with aerosol flow synthesized B, N-codoped TiO_2 hollow spheres. J. Hazard. Mater. 190, 604–612. https://doi.org/10.1016/j.jhazmat.2011.03.099

Dobrucka, R. (2018). Synthesis of MgO nanoparticles using artemisia abrotanum herba extract and their antioxidant and photocatalytic properties. Iran J. Sci. Tchnol. A 42, 547–555. https://doi.org/10.1007/s40995-016-0076-x

Essien, E.R., Atasie, V.N., Okeafor, A.O., Nwude, D.O. (2020). Biogenic synthesis of magnesium oxide nanoparticles using Manihot esculenta (Crantz) leaf extract. Int. Nano Lett. 10, 43–48. https://doi.org/10.1007/s40089-019-00290-w

Fenelon, E., Bui, D.P., Tran, H.H., You, S.J., Wang, Y.F., Cao, T.M., Van Pham, V. (2020). Straightforward Synthesis of SnO_2/Bi_2S_3/BiOCl–$Bi_{24}O_{31}Cl_{10}$ composites for drastically enhancing rhodamine B photocatalytic degradation under visible light. ACS Omega 5, 20438–20449. https://doi.org/10.1021/acsomega.0c02461

Fenelon, E., Hussain, A., Yang, T.H., Chang, G.M., Chen, S.W., Wei, R.J., You, S.J., Wang, Y.F. (2019). High photocatalyst module on degradation of extracted gas from soil under visible light. Aerosol Air Qual. Res. 19, 2865–2878. https://doi.org/10.4209/aaqr.2019.10.0499

Feng, H., Xu, H., Feng, H., Gao, Y., Jin, X. (2019). The sol-gel synthesis and photocatalytic activity of Gd-SiO_2-TiO_2 photocatalyst. Chem. Phys. Lett. 733, 136676. https://doi.org/10.1016/j.cplett.2019.136676

Fujiwara, K., Müller, U., Pratsinis, S.E. (2016). Pd subnano-clusters on TiO_2 for solar-light removal of NO. ACS Catal. 6, 1887–1893. https://doi.org/10.1021/acscatal.5b02685

Gao, D.Z., Watkins, M.B., Shluger, A.L. (2012). Transient mobility mechanisms of deposited metal atoms on insulating surfaces: Pd on MgO (100). J. Phys. Chem. C 116, 14471–14479. https://doi.org/10.1021/jp303951y

Guan, M., Xiao, C., Zhang, J., Fan, S., An, R., Cheng, Q., Xie, J., Zhou, M., Ye, B., Xie, Y. (2013). Vacancy Associates promoting solar-driven photocatalytic activity of ultrathin bismuth oxychloride nanosheets. J. Am. Chem. Soc. 135, 10411–10417. https://doi.org/10.1021/ja402956f

Guo, D., Hu, C., Zhang, C. (2013). First-principles study on doping and temperature dependence of thermoelectric property of Bi2S3 thermoelectric material. Mater. Res. Bull. 48, 1984–1988. https://doi.org/10.1016/j.materresbull.2013.02.004

Guo, Y., Zhang, G., Gan, H., Zhang, Y. (2012). Micro/nano-structured $CaWO_4/Bi_2WO_6$ composite: Synthesis, characterization and photocatalytic properties for degradation of organic contaminants. Dalton Trans. 41, 12697–12703. https://doi.org/10.1039/C2DT31376F

Huang, Y., Cao, J.J., Kang, F., You, S.J., Chang, C.W., Wang, Y.F. (2017). High selectivity of visible-light-driven La-doped TiO_2 photocatalysts for NO removal. Aerosol Air Qual. Res. 17, 2555–2565. https://doi.org/10.4209/aaqr.2017.08.0282

Huy, T.H., Phat, B., Thi, C.M., Viet, P.V. (2018). High photocatalytic removal of NO gas over SnO_2 nanoparticles under solar light. Environ. Chem. Lett. 17, 527–531. https://doi.org/10.1007/s10311-018-0801-0

Jayachandhiran, A., Raj, D., Alphonse, A.A. (2017). Solvent effects on the properties of Bi_2S_3 nanoparticles: Photocatalytic application. J. Mater. Sci.: Mater. Electron. 28, 3487–3494. https://doi.org/10.1007/s10854-016-5947-6

John, P., Johari, K., Gnanasundaram, N., Appusamy, A., Thanabalan, M. (2021). Enhanced photocatalytic performance of visible light driven TiO_2/g-C_3N_4 for degradation of diclofenac in aqueous solution. Environ. Technol. Innovation 22, 101412. https://doi.org/10.1016/j.eti.2021.101412

Lei, Y., Wang, G., Song, S., Fan, W., Zhang, H. (2009). Synthesis, characterization and assembly of BiOCl nanostructure and their photocatalytic properties. CrystEngComm. 11, 1857–1862. https://doi.org/10.1039/B909013B

Li, D.B., Hu, L., Xie, Y., Niu, G., Liu, T., Zhou, Y., Gao, L., Yang, B., Tang, J. (2016). Low-temperature-processed amorphous Bi_2S_3 film as an inorganic electron transport layer for perovskite solar cells. ACS Photonics 3, 2122–2128. https://doi.org/10.1021/acsphotonics.6b00582

Li, J., Zhang, W., Ran, M., Sun, Y., Huang, H., Dong, F. (2019). Synergistic integration of Bi metal and phosphate defects on hexagonal and monoclinic $BiPO_4$: Enhanced photocatalysis and reaction mechanism. Appl. Catal. B 243, 313–321. https://doi.org/10.1016/j.apcatb.2018.10.055

Li, Y., Zhao, H., Wu, Y. (2015). Characteristics of particulate matter during haze and fog (pollution) episodes over northeast China, Autumn 2013. Aerosol and Air Qual. Res. 15, 853–864. https://doi.org/10.4209/aaqr.2014.08.0158

Liu, L., Zheng, C., Qu, R., Wang, J., Liu, X., Wu, W., Gao, X. (2019). Non-thermal plasma assisted preparation of $MnCeO_x$, MnO_x and CeO_2 catalysts for enhancement of surface active oxygen and NO oxidation activity. Aerosol Air Qual. Res. 19, 945–958. https://doi.org/10.4209/aaqr.2018.12.0456

Long, L.L., Zhang, A.Y., Huang, Y.X., Zhang, X., Yu, H.Q. (2015). A robust cocatalyst Pd_4S uniformly anchored onto Bi_2S_3 nanorods for enhanced visible light photocatalysis. J. Mater. Chem. A 3, 4301–4306. https://doi.org/10.1039/C4TA05818F

Neves, T.M., Frantz, T.S., do Schenque, E.C.C., Gelesky, M.A., Mortola, V.B. (2017). An investigation into an alternative photocatalyst based on CeO_2/Al_2O_3 in dye degradation. Environ. Technol. Innovation 8, 349–359. https://doi.org/10.1016/j.eti.2017.08.003

Nguyen, S.N., Truong, T.K., You, S.J., Wang, Y.F., Cao, T.M., Pham, V. V. (2019). Investigation on photocatalytic removal of NO under visible light over Cr-doped ZnO nanoparticles. ACS Omega 4, 12853–12859. https://doi.org/10.1021/acsomega.9b01628

Nie, G., Lu, X., Lei, J., Yang, L., Wang, C. (2015). Facile and controlled synthesis of bismuth sulfide nanorods-reduced graphene oxide composites with enhanced supercapacitor performance. Electrochim. Acta 154, 24–30. https://doi.org/10.1016/j.electacta.2014.12.090

Pham, M.T., Bui, D.P., Lin, I.F., Phuong, N.H., Huang, Y., Cao, J., You, S.J., Wang, Y.F. (2020). Enhanced near-visible-light photocatalytic removal of formaldehyde over Au-assisted $ZnSn(OH)_6$ microcubes. Environ. Technol. Innovation 20, 101112. https://doi.org/10.1016/j.eti.2020.101112

Pham, M.T., Hussain, A., Bui, D.P., Nguyen, T.M.T., You, S.J., Wang, Y.F. (2021). Surface plasmon resonance enhanced photocatalysis of Ag nanoparticles-decorated Bi_2S_3 nanorods for NO degradation. Environ. Technol. Innovation 23, 101755. https://doi.org/10.1016/j.eti.2021.101755

Seddigi, Z.S., Gondal, M.A., Baig, U., Ahmed, S.A., Abdulaziz, M.A., Danish, E.Y., Khaled, M.M., Lais, A. (2017). Facile synthesis of light harvesting semiconductor bismuth oxychloride nano photo-catalysts for efficient removal of hazardous organic pollutants. PLoS ONE 12, e0172218. https://doi.org/10.1371/journal.pone.0172218

Sun, B., Dong, J., Shi, W.J., Ai, S.Y. (2016). A hierarchical charge transport cascade based on W-Bi_2S_3/poly(thiophenyl-3-boronic acid) hybrid for robust photoelectrochemical analysis of subgroup J of avian leukosis virus. Sens. Actuators, B 229, 75–81. https://doi.org/10.1016/j.snb.2016.01.063

Sun, Y., Liao, J., Dong, F., Wu, S., Sun, L. (2019). A Bi/BiOI/$(BiO)_2CO_3$ heterostructure for enhanced photocatalytic NO removal under visible light. Chinese J. Catal. 40, 362–370. https://doi.org/10.1016/S1872-2067(18)63187-0

Trapalis, A., Todorova, N., Giannakopoulou, T., Boukos, N., Speliotis, T., Dimotikali, D., Yu, J. (2016). TiO_2/graphene composite photocatalysts for NO_x removal: A comparison of surfactant-stabilized graphene and reduced graphene oxide. Appl. Catal., B 180, 637–647. https://doi.org/10.1016/j.apcatb.2015.07.009

Viswanatha, R., Venkatesh, T., Vidyasagar, C., Nayaka, Y.A. (2012). Preparation and characterization of ZnO and Mg-ZnO nanoparticle. Arch. Appl. Sci. Res. 4, 480–486.

Wang, G., Zhang, R., Gomez, M.E., Yang, L., Levy Zamora, M., Hu, M., Lin, Y., Peng, J., Guo, S., Meng, J., Li, J., Cheng, C., Hu, T., Ren, Y., Wang, Yuesi, Gao, J., Cao, J., An, Z., Zhou, W., Li, G., *et al.* (2016). Persistent sulfate formation from London Fog to Chinese haze. Proc. Natl. Acad. Sci. U.S.A. 113, 13630–13635. https://doi.org/10.1073/pnas.1616540113

Wang, Q., Zhou, J., Zhang, J., Zhu, H., Feng, Y., Jin, J. (2020). Effect of ceria doping on catalytic activity and SO_2 resistance of MnO_x /TiO_2 catalysts for selective catalytic reduction of NO with NH_3 at low temperature. Aerosol Air Qual. Res. 20, 477–488. https://doi.org/10.4209/aaqr.2019.10.0546

Yan, J., Zhou, F., Zhou, Y., Wu, X., Zhu, Q., Liu, H., Lu, H. (2018). Wet oxidation and absorption procedure for NO_x removal. Environ. Technol. Innovation 11, 41–48. https://doi.org/10.1016/j.eti.2018.03.006

Yu, C., Wang, H., Lu, M., Zhu, F., Yang, Y., Huang, H., Zou, C., Xiong, J., Zhong, Z. (2020). Agricultural waste derived catalysts for low temperature SCR process: Optimization of preparation process, catalytic activity and characterization. Aerosol Air Qual. Res. 20, 862–876. https://doi.org/10.4209/aaqr.2019.11.0596

Zhang, B., Chen, D., Liu, H., Zou, X., Chen, T. (2020). Selective catalytic reduction of NO with NH_3 over high purity palygorskite-supported MnO_2 with different crystal structures. Aerosol Air Qual. Res. 20, 1155–1165. https://doi.org/10.4209/aaqr.2020.03.0099

Zhang, X., Wang, X.B., Wang, L.W., Wang, W.K., Long, L.L., Li, W.W., Yu, H.Q. (2014). Synthesis of a highly efficient BiOCl single-crystal nanodisk photocatalyst with exposing {001} facets. ACS Appl. Mater. Inter. 6, 7766–7772. https://doi.org/10.1021/am5010392

Zhao, G., Zheng, Y., He, Z., Lu, Z., Wang, L., Li, C., Jiao, F., Deng, C. (2018). Synthesis of Bi_2S_3 microsphere and its efficient photocatalytic activity under visible-light irradiation. Trans. Nonferrous Met. Soc. China 28, 2002–2010. https://doi.org/10.1016/S1003-6326(18)64844-7

Zhao, M., Xiu, G., Qiao, T., Li, Y., Yu, J. (2016). Characteristics of haze pollution episodes and analysis of a typical winter haze process in Shanghai. Aerosol and Air Qual. Res. 16, 1625–1637. https://doi.org/10.4209/aaqr.2016.01.0049

Zhu, Y., Zhu, R., Zhu, G., Wang, M., Chen, Y., Xi, Y., He, H. (2017). Plasmonic Ag coated Zn/Ti-LDH with excellent photocatalytic activity. Appl. Surf. Sci. 433, 458–467. https://doi.org/10.1016/j.apsusc.2017.09.236